Using the Cluster-Plus-Glue-Atom model to design the composition of low Young's modulus β-Ti alloys for orthopaedic applications

Noluntu Muchavi[1,2], *Lerato* Raganya[1] and *Elizabeth* Makhatha[2]

[1] Advanced Materials and Engineering, Manufacturing Cluster, Council for Scientific and Industrial Research, Pretoria, South Africa
[2]Department of Metallurgy, School of Mining, Metallurgy and Chemical Engineering, University of Johannesburg, Doornfontein Campus, Johannesburg, 2028, South Africa

Abstract. The design and development of metastable β-type Ti alloys with low Young's moduli (E) requires the use of multiple β-phase stabilising alloying elements. The most commonly used alloy development design strategies do not provide accurate composition design. Moreover, the process of developing alloys is still based on empirical exploration, which is costly and time consuming. In this study, the cluster-plus-glue-atom (CPGA) model was employed in the composition design and interpretation of low-E, β-type Ti based alloys. Microstructure, phase analysis, Young's modulus (mechanical testing and nano-indentation testing) of the as-cast alloys were investigated. The results demonstrated that the CPGA model was effective in formulating compositions which were able to simultaneously achieve high β-phase stability and low-E as exemplified by the $[(Mo_{0.4}Sn_{0.6})\ (Ti)_{14}]\ (Nb)_1$ alloy which obtained a Young's modulus of 59 GPa.

*Corresponding authors: muchavinola@gmail.com and EMakhatha@uj.ac.za

1 Introduction

Surgical stainless steel (316L), cobalt-chromium (Co-Cr) alloys, and titanium (Ti) alloys are commonly used biomaterials for orthopaedic and dental implants [1–3]. Titanium and its alloys, specifically, are chosen for orthopaedic implants due to their excellent resistance to corrosion and fatigue, biocompatibility, mechanical properties, and lower elasticity compared to other materials [4–6]. Stainless steel materials are favoured for their affordability, availability, processability, and good biocompatibility. Cobalt-chromium alloys, on the other hand, offer superior wear resistance, corrosion resistance, and fatigue strength [7]. The use of 316L stainless steel and Co-Cr alloys in orthopedic applications is constrained by the potential release of nickel (Ni), cobalt (Co), and chromium (Cr) due to corrosion and wear. Studies indicate that Ni can lead to skin conditions like dermatitis, while

Co has been linked to neurological problems in some patients after years of implantation. Moreover, Cr can initiate oxidative processes in the body that may damage the kidneys, liver, and blood cells. Additionally, the Young's modulus of Co-Cr alloys and 316L stainless steel is considerably higher—240 GPa for Co-Cr alloys and 210 GPa for 316L stainless steel—compared to human bone, which ranges from 10 to 30 GPa, this disparity can result in a stress-shielding effect [7–9].

While titanium alloys, especially Ti-6Al-4V, are commonly preferred for orthopaedic applications, they do have certain drawbacks. The Young's modulus of Ti-6Al-4V (≈ 110 GPa) is considerably higher than that of human bone (10-30 GPa) [10–12]. Additionally, there have been observations of the release of vanadium (V) and aluminium (Al) ions from Ti-6Al-4V in the human body, which limits its biomedical applications [13, 14]. Research suggests that the release of trace amounts of vanadium (V) and aluminum (Al) in the human body can lead to cytotoxic effects and neurological disorders, including Alzheimer's disease[15]. Additionally, the Young's modulus of the α + β Ti6Al4V alloy is greater than that of β-type titanium alloys [14, 16]. To overcome these limitations, researchers have focused on developing new Ti-based alloys that incorporate non-toxic β-stabilizing alloying elements such as Molybdenum, Niobium, Tantalum, Tin, Chromium etc. to achieve a high β-phase stability and a low Young's modulus [14], [16–19].

To simultaneously achieve a low Young's modulus and a highly stable β phase necessitates the incorporation of multiple alloying elements [19]–[21]. In the field of multicomponent alloy design, various methods have been employed to guide the selection of alloy compositions. Among these methods are the d-electron concept [20], Mo-equivalence (Moeq) [21], and electron concentration criterion (e/a) [22]. While these techniques have been widely used, they often fall short in terms of providing precise composition design. As a result, the development of alloys still heavily relies on empirical exploration and a trial-and-error approach [22]. Also, the inclusion of numerous elements brings about composition complexity, making the design process more intricate [20].

To address this complexity and facilitate the development of new alloys, Dong *et.al* [23] developed the cluster-plus-glue-atom (CPGA) model for body-centered cubic (BCC) alloys, shown in Figure 1, as an effective design approach. It introduces a novel framework of alloy design by incorporating the concept of clusters and glue atoms, taking into account the arrangement of atoms within the alloy structure and their interactions. This model provides the basic compositional and structural information of a material through its cluster formula [(center atom) -(shell atoms)$_{14}$] (glue atoms)$_{1\text{-}8}$]. The elements are positioned within the formula based on their interactions, characterized by their enthalpy of mixing (ΔH). Elements with a negative ΔH, such as Mo (-4 kJ/mol) and Sn (-21 kJ/mol), are preferentially placed at the cluster centre. Elements with a positive ΔH, like Nb (2 kJ/mol), are assigned to the glue site. Elements with a ΔH of zero (0), such as Ti (0 kJ/mol), are positioned in the cluster shell. By appropriately arranging the alloying elements within the cluster formula, the CPGA model enables the design of alloys with high β phase stability and a low Young's modulus. This approach helps mitigate the challenges associated with composition complexity in multi-component systems [21], [24–27]. Researchers and engineers can streamline the alloy design process, reduce the reliance on empirical exploration, and enhance the accuracy of composition design by utilising the CPGA model. This model represents a significant advancement in the field of multicomponent alloy design, offering a more efficient and precise approach to optimise alloy compositions for various applications. In this paper, the

CPGA model with cluster formula $[(Mo_{1-x},Sn_x)(Ti)_{14}](Nb)_1$ was used to design low Young's modulus β-Ti Alloys for orthopaedic applications.

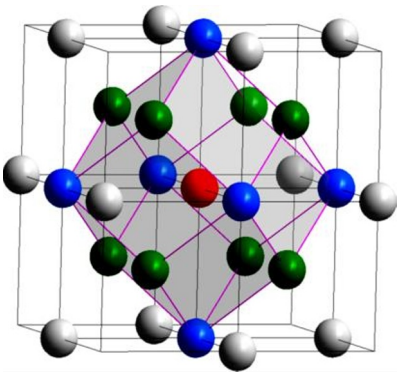

Fig. 1: Geometrical configuration of the cluster-plus-glue-atom model for BCC structure [22]. It consists of eight green atoms of the 1st-neighbor shell and six blue atoms of the 2nd-neighbor shell. The red represents the cluster centre atom, and the grey are the glue atoms.

2 Methodology

2.1 Starting materials

The materials used in this study were angular shaped Ti and Nb powder with particles sizes of -45 and -5 µm respectively, spherically shaped Mo and Sn powder with particles sizes of -150 µm. The Ti and Nb powders were provided by Thermo Scientific (SA), while the Sn and Mo powders were sourced from Alfa Aesar (USA).

2.2 Alloy design and fabrication

The CPGA model which arranges alloying elements within the cluster formula thus providing chemical compositions of highly stable β phase alloys with low Young's modulus was employed to formulate chemical compositions (Table 1) for alloys to be used in this study. 100 g of powders per alloy were weighed using an Ohaus EX 224 balance. The powders were subsequently mixed and compacted into green compacts with a diameter of 45 mm using a uniaxial cold compacting machine at a pressure of 250 bars. The compacted samples were subsequently melted in an arc furnace using a non-consumable tungsten electrode and a water-cooled copper crucible, all within an argon atmosphere. Ti getters were employed to minimize oxidation during the process. To ensure homogeneity, the samples were inverted and re-melted five times.

Table 1: Chemical composition of the starting alloys.

Cluster formula	***Composition (wt.%)***
$[(Mo_{0.8}Sn_{0.2})\ (Ti)_{14}]\ (Nb)_1$	Ti-8.9Mo-10.8Nb-2.7Sn
$[(Mo_{0.75}Sn_{0.25})\ (Ti)_{14}]\ (Nb)_1$	Ti-8.3Mo-10.7Nb-3.4Sn
$[(Mo_{0.4}Sn_{0.6})\ (Ti)_{14}]\ (Nb)_1$	Ti-4.4Mo-10.6Nb-8.2Sn

2.3 Microstructure, chemical composition and phase analysis

To analyze the microstructure of the samples, a Leica DMI 5000M optical microscope was employed. Precision-cut samples from the as-cast ingots were mounted, ground, and polished according to the ASTM E3-11 standard guide for metallographic specimen preparation. For final polishing, colloidal silica (3 μm) was used. The samples were etched with Kroll's reagent, consisting of 3 ml HNO3, 2 ml HF, and 100 ml distilled water. Phase identification was conducted using a PANalytical Empyrean diffractometer system. The system operated at 45 kV and 40 mA, with Cu Kα as the X-ray source, having λ1 = 0.1540598 nm and λ2 = 1.544426 nm. The scan range for the diffraction analysis was set from 20 to 90 degrees 2θ.

2.4 Mechanical testing

Tensile testing was carried out using an Instron 1342 mechanical testing machine. The dimensions of the tensile specimen are illustrated in Figure 2. The testing was conducted at a speed of 0.5 mm/sec, and three test specimens were tested for each alloy. The elastic modulus of the alloys was determined using an AntonPaar TTXNHT3 nano-indenter following the ASTM D785 standard. The nano-indenter was operated with an applied load of 400mN, a penetration time of 20 seconds, a holding time of 20 seconds, and a releasing time of 20 seconds. An average of five tests per sample was conducted to obtain accurate measurements.

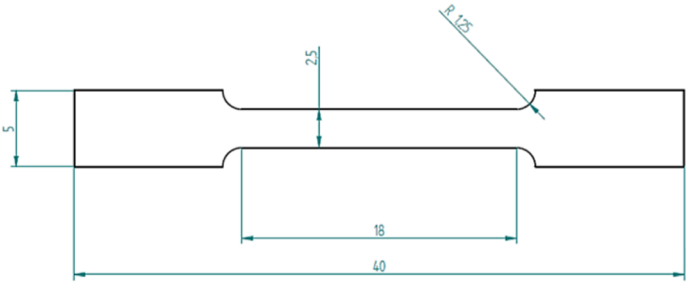

Fig. 2: Schematic dimensions of the tensile specimen.

3 Results

3.1 Microstructure, chemical composition, and phase analysis

Optical images of the microstructures of the alloys are depicted in Figure 3. All the alloys exhibited large equiaxed β grains without any signs of secondary phases. The microstructure of the $[(Mo_{0.75}Sn_{0.25})(Ti)_{14}](Nb)_1$ and $[(Mo_{0.4}Sn_{0.6})(Ti)_{14}](Nb)_1$ (Figure 2 b and c) revealed sub-grain structures within the primary grains when etched. The presence of such structures in titanium alloys is commonly associated with the recovery of work-hardened alloys [21]; however, they have also been observed in as-cast metastable β-type Ti alloys, likely due to compositional variations [28-29] as alloying elements such as Mo, Nb and Sn are known to effortlessly segregate during the solidification process in Ti alloys [30–34].

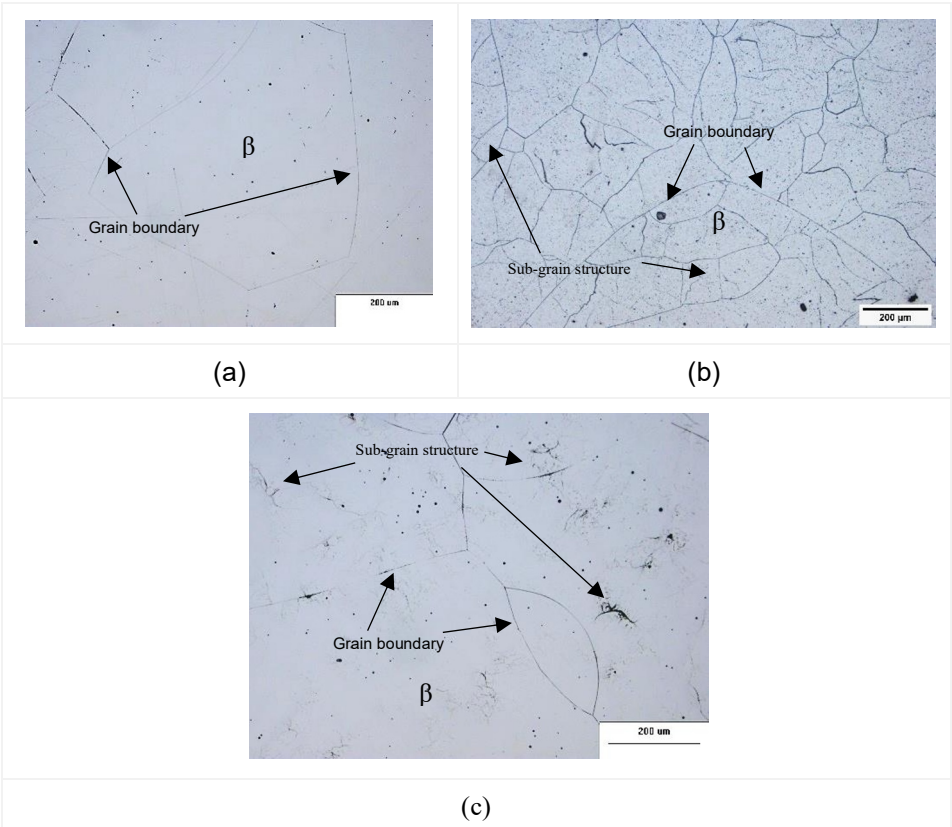

Fig. 3: Optical micrographs of the alloys (a) [$(Mo_{0.8}Sn_{0.2})$ $(Ti)_{14}$] $(Nb)_1$], (b) [$(Mo_{0.75}Sn_{0.25})$ $(Ti)_{14}$] $(Nb)_1$ and (c) [$(Mo_{0.4}Sn_{0.6})$ $(Ti)_{14}$] $(Nb)_1$. x100.

3.2 XRD analysis

The X-ray diffraction patterns obtained from the alloys are depicted in Figure 4. The alloys [$(Mo_{0.8}Sn_{0.2})$ $(Ti)_{14}$] $(Nb)_1$ and [$(Mo_{0.75}Sn_{0.25})$ $(Ti)_{14}$] $(Nb)_1$ exhibited diffraction peaks associated with the β phase. However, the alloy [$(Mo_{0.4}Sn_{0.6})$ $(Ti)_{14}$] $(Nb)_1$ displayed diffraction peaks corresponding to both the β phase and the secondary martensitic α″ phase. It is important to note that due to the rapid solidification and cooling resulting from solidification in the copper mold, the final microstructure is anticipated to consist of metastable phases [21]. The formation of the observed secondary phase is said to form via a co-operative shear of atoms from the β phase and is seen in rapidly cooled alloys [35, 36] containing a lean concentration of β stabilizing elements [37]. The presence of the α″ phase depends on the proportion of β stabilizing elements, as suggested by [37-38]. The results demonstrate that the substitution of 0.6 Mo atoms with Sn atoms resulted in the destabilization of the β phase. This observation can be attributed to the relative effectiveness of Mo as a β phase stabilizer compared to Sn. It can be inferred that the presence of higher amounts of Sn in the alloy contributed to a reduced stabilization effect on the β phase, leading to its destabilization hence the formation of the secondary martensitic α″ phase.

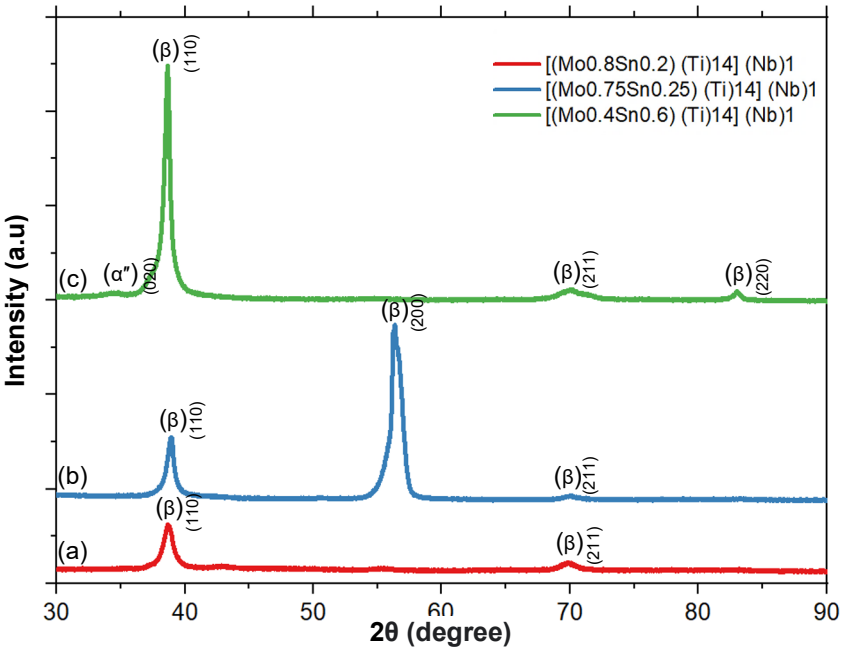

Fig. 4: XRD patters of the alloys (a) [$(Mo_{0.8}Sn_{0.2})$ $(Ti)_{14}$] (Nb)], (b) [$(Mo_{0.75}Sn_{0.25})$ $(Ti)_{14}$] $(Nb)_1$ and (c) [$(Mo_{0.4}Sn_{0.6})$ $(Ti)_{14}$] $(Nb)_1$.

3.3 Mechanical testing

Figures 5 and 6 show the tensile strength and elastic modulus of the alloys respectively. The results show that the [$(Mo_{0.8}Sn_{0.2})$ $(Ti)_{14}$] $(Nb)_1$ and the [$(Mo_{0.4}Sn_{0.6})$ $(Ti)_{14}$] $(Nb)_1$ alloys had similar tensile strengths with averages of 540 and 578 MPa respectively. The tensile strength of the [$(Mo_{0.75}Sn_{0.25})$ $(Ti)_{14}$] $(Nb)_1$ had an average of 401 MPa. However, the overlapping error bars on all samples indicate that there were no significant differences in the tensile strength.

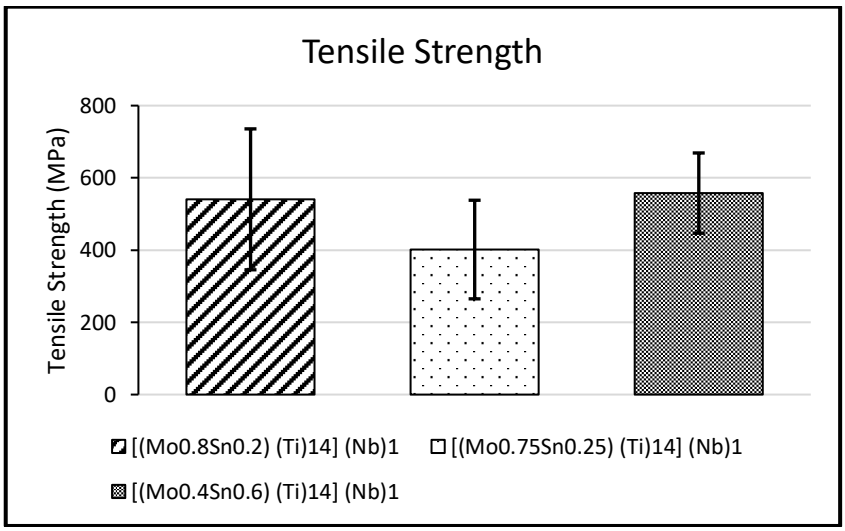

Fig. 5: Tensile results of the designed alloys.

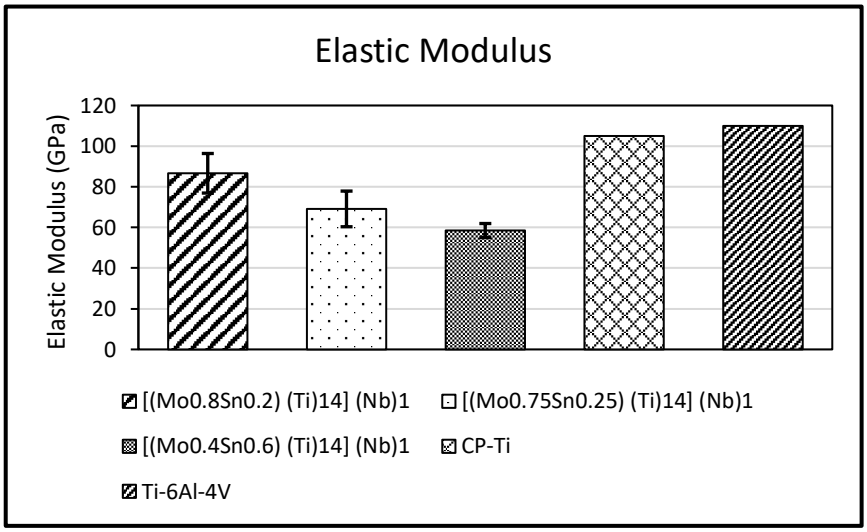

Fig. 6: Young's modulus of the designed alloys along with those of CP-Ti and Ti6Al4V found in literature for comparion purposes.

The determined elastic moduli of all the formulated alloys were found to be lower compared to both commercially favoured Ti6Al4V (110 GPa) orthopaedic alloys and CP-Ti (105 GPa) [39]. Specifically, the $[(Mo_{0.8}Sn_{0.2})\ (Ti)_{14}]\ (Nb)_1$ alloy exhibited an elastic modulus of 87 GPa. Notably, an increase in the Sn atom content from 0.2 to 0.25 within the cluster formula resulted in a decrease in the elastic modulus from 87 GPa to 69 GPa. Subsequently, a further increase in Sn atom content to 0.6 yielded an even lower elastic modulus of 59 GPa, as observed in the $[(Mo_{0.4}Sn_{0.6})\ (Ti)_{14}]\ (Nb)_1$ alloy. The observed elastic modulus of 59 GPa in the $[(Mo_{0.4}Sn_{0.6})\ (Ti)_{14}]\ (Nb)_1$ alloy was not expected since this alloy contained minor volume fractions of the α″ phase which has been said to increase the elastic modulus of β-Ti alloys since the elastic modulus of the α″ phase is higher than that of the β phase [11, 20, 40]. However, contrary to these expectations, previous studies by researchers such as [25,37], [38], have reported a lower elastic modulus in alloys containing the secondary α″ phase compared to those composed entirely of the β phase. Their results also indicated that their alloys contained minor fractions of the ω phase which is said has the highest elastic modulus amongst all these phases [40-41]. It is possible that the volume fraction of the ω phase was higher in the alloys which comprised of the β phase hence the higher elastic modulus. In this work, the XRD analysis was unable to detect the ω phase which has been said to be difficult to detect without the use of slow scanning speeds [38]. Further phase analysis methods such as electron backscatter diffraction (EBSD) or transmission electron microscopy (TEM) are required to confirm if this was also the case in the studied alloys.

The nanoindentation load-displacement curves of the designed alloys subjected to indentation loads of 400 mN are presented in Figure 7 with the results given in Table 2. From the figure, it can be seen that the alloys exhibit similar loading and unloading behaviours that are smooth with no pop-in effect. The load-displacement curves show that the $[(Mo_{0.8}Sn_{0.2})\ (Ti)_{14}]\ (Nb)_1$ alloy had a low penetration depth, that is, the indenter does not penetrate easily into the material. This resistance can be attributed to the stiffness of the alloy, which is indicative of its high modulus (82 GPa). The addition of 0.25 and 0.6 Atoms of Sn into the cluster formula, substituting the Mo atoms, resulted in an increase in the depth of penetration as evidenced by the unloading curves shifting to the right thus indicating softening of the alloys which translates to a decrease in elastic modulus where the values for the

$[(Mo_{0.75}Sn_{0.25})\ (Ti)_{14}]\ (Nb)_1$ and $[(Mo_{0.4}Sn_{0.6})\ (Ti)_{14}]\ (Nb)_1$ were 73 and 68 GPa, respectively. The trend observed in the elastic modulus values from the nano-indentation correlates with that obtained from mechanical testing where the increase in the number of Sn atoms (wt.% Sn) resulted in a decrease in the Young's modulus. Several studies have reported the reduction in elastic modulus of β-type titanium alloys by incorporating Sn as an alloying element. Xie *et.al* [42] investigated the effect of Sn addition on Ti-Nb-Sn alloys. Similarly, Hao *et.al* [43] studied the impact of Sn in Ti-Nb-Zr-Sn alloys. Additionally, Zhang *et.*al [44] examined the influence of Sn in Ti-Nb-Mo-Sn alloys, while another study by Moraes *et.*al [38] focused on Ti-Nb-Sn alloys. In all these investigations, the common finding was a decrease in the elastic modulus of the alloys due to the addition and increase of Sn.

Table 2: Nano-indentation elastic modulus of the alloys.

Cluster formula	***Elastic Modulus (E) (GPa)***
$[(Mo_{0.8}Sn_{0.2})\ (Ti)_{14}]\ (Nb)_1$	82
$[(Mo_{0.75}Sn_{0.25})\ (Ti)_{14}]\ (Nb)_1$	73
$[(Mo_{0.4}Sn_{0.6})\ (Ti)_{14}]\ (Nb)_1$	68

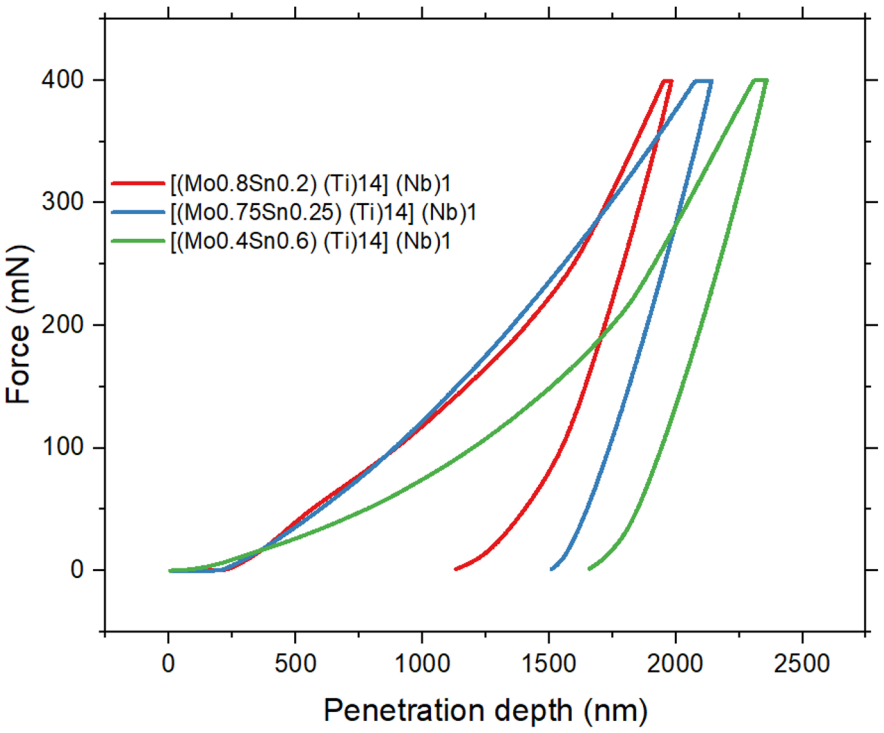

Fig. 7: Nano-indentation elastic modulus of the alloys.

4 Conclusions and future work

In this study, the CPGA model with cluster formula $[(Mo_{1-x},Sn_x)(Ti)_{14}](Nb)_1$ was used to design low Young's modulus β-Ti Alloys for orthopaedic applications.

- The alloys formulated in this study were found to exhibit microstructures consisting of equiaxed β grains, and no evidence of secondary phases was observed.
- X-ray diffraction (XRD) analysis was conducted to investigate the structural characteristics resulting from the substitution of 0.25 and 0.6 atoms of Mo with Sn in the cluster shell. The analysis revealed the presence of minute secondary α″ phases, suggesting that the addition of Sn led to the formation of these secondary phases within the alloy structure.
- Mechanical testing and nano-indentation results consistently indicated that the elastic modulus of the alloys was lower compared to the conventional orthopaedic implants which can be advantageous for orthopaedic applications by potentially reducing stress shielding effects and improving biomechanical compatibility.
- The CPGA (Cluster-plus-Glue-Atom) model was utilized in this study to design multi-alloy compositions that exhibit high β-phase stability and a low elastic modulus. The model proved to be effective in achieving this objective by optimising the alloy compositions. Among the tested compositions, the $[(Mo_{0.4}Sn_{0.6})\ (Ti)_{14}]\ (Nb)_1$ alloy exhibited the lowest elastic modulus, with a value of 59 GPa.
- Future work will be undertaken to study the influence of increased Sn on the $[(Mo_{1-x}Sn_x)\ (Ti)_{14}]\ (Nb)_1$ alloy to see if the elastic modulus can be further decreased.
- Phase analysis using EBSD an TEM will be undertaken to analyse and study the ω phase if present in the alloys.

This research was financially supported by the Titanium Centre of Competence (TiCoC), the Council for Scientific and Industrial Research (CSIR) and the Department of Science and Innovation (DSI).

References

[1] P. S. Nnamchi, R. E. Njoku, and O. A. Fasuba, "Alloy design and property evaluation of Ti-Mo-Nb-Sn for biomedical applications," 2013. [Online]. Available: www.nijotech.com

[2] K. Prasad *et al.*, "Metallic biomaterials: Current challenges and opportunities," *Materials*, vol. 10, no. 8. MDPI AG, Jul. 31, 2017. doi: 10.3390/ma10080884.

[3] M. Bahraminasab, M. B. Nasab, and M. R. Hassan, "Metallic Biomaterials of Knee and Hip-A Review," 2010. [Online]. Available: http://www.sbaoi.org

[4] S. Li and T. hyun Nam, "Superelasticity and tensile strength of Ti-Zr-Nb-Sn alloys with high Zr content for biomedical applications," *Intermetallics (Barking)*, vol. 112, no. June, p. 106545, 2019, doi: 10.1016/j.intermet.2019.106545.

[5] A. R. Vieira Nunes, S. Borborema, L. S. Araújo, L. Malet, J. Dille, and L. Henrique de Almeida, "Influence of thermo-mechanical processing on structure and mechanical properties of a new metastable β Ti–29Nb–2Mo–6Zr alloy with low Young's modulus," *J Alloys Compd*, vol. 820, p. 153078, 2020, doi: 10.1016/j.jallcom.2019.153078.

[6] A. Dehghan-Manshadi, D. Kent, D. StJohn, and M. Dargusch, "Properties of Powder Metallurgy-Fabricated Oxygen-Containing Beta Ti–Nb–Mo–Sn–Fe Alloys for Biomedical Applications," *Adv Eng Mater*, vol. 22, no. 3, pp. 1–6, 2020, doi: 10.1002/adem.201901229.

[7] K. S. Katti, "Biomaterials in total joint replacement," *Colloids Surf B Biointerfaces*, vol. 39, no. 3, pp. 133–142, Dec. 2004, doi: 10.1016/j.colsurfb.2003.12.002.

[8] M. Kaur and K. Singh, "Review on titanium and titanium based alloys as biomaterials for orthopaedic applications," *Materials Science and Engineering C*, vol. 102. Elsevier Ltd, pp. 844–862, Sep. 01, 2019. doi: 10.1016/j.msec.2019.04.064.

[9] H. N. Yu, H. C. Hsu, S. C. Wu, S. K. Hsu, and W. F. Ho, "Structure and mechanical properties of as-cast Ti-5Sn-xMo alloys," *Materials*, vol. 10, no. 5, 2017, doi: 10.3390/ma10050458.

[10] M. Niinomi, "Design and development of metallic biomaterials with biological and mechanical biocompatibility," *Journal of Biomedical Materials Research - Part A*, vol. 107, no. 5. John Wiley and Sons Inc., pp. 944–954, May 01, 2019. doi: 10.1002/jbm.a.36667.

[11] R. Jha and G. S. Dulikravich, "Discovery of new Ti-based alloys aimed at avoiding/minimizing formation of α" and ω-phase using calphad and artificial intelligence," *Metals (Basel)*, vol. 11, no. 1, pp. 1–15, Jan. 2021, doi: 10.3390/met11010015.

[12] Y. Qu *et al.*, "Ti-24Nb-4Zr-8Sn Alloy Pedicle Screw Improves Internal Vertebral Fixation by Reducing Stress-Shielding Effects in a Porcine Model," *Biomed Res Int*, vol. 2018, 2018, doi: 10.1155/2018/8639648.

[13] A. Raquel, V. Nunes, S. Borborema, C. Angelo, and L. Sales, "Microstructure and Mechanical Properties of Ti-12Mo-8Nb Alloy Hot Swaged and Treated for Orthopedic Applications," vol. 20, pp. 526–531, 2017.

[14] A. Dehghan-Manshadi, D. Kent, D. StJohn, and M. Dargusch, "Properties of Powder Metallurgy-Fabricated Oxygen-Containing Beta Ti–Nb–Mo–Sn–Fe Alloys for Biomedical Applications," *Adv Eng Mater*, vol. 22, no. 3, Mar. 2020, doi: 10.1002/adem.201901229.

[15] N. Moshokoa, L. Raganya, B. Obadele, P. Olubambi, and R. Machaka, "Effects of Mo content on the microstructural and mechanical properties of as-cast Ti-Mo alloys," in *IOP Conference Series: Materials Science and Engineering*, Institute of Physics Publishing, Nov. 2019. doi: 10.1088/1757-899X/655/1/012015.

[16] M. Nakai, M. Niinomi, X. Zhao, and X. Zhao, "Self-adjustment of Young's modulus in biomedical titanium alloys during orthopaedic operation," *Mater Lett*, vol. 65, no. 4, pp. 688–690, Feb. 2011, doi: 10.1016/j.matlet.2010.11.006.

[17] D. C. Zhang, S. Yang, M. Wei, Y. F. Mao, C. G. Tan, and J. G. Lin, "Effect of Sn addition on the microstructure and superelasticity in Ti-Nb-Mo-Sn Alloys," *J Mech Behav Biomed Mater*, vol. 13, pp. 156–165, Sep. 2012, doi: 10.1016/j.jmbbm.2012.04.017.

[18] F. Ahmad, H. Zuhailawati, and F. N. Ahmad, "A Brief Review on the Properties of Titanium as a Metallic Biomaterials," *International Journal of Electroactive Materials*, pp. 63–67, 2020, [Online]. Available: https://www.researchgate.net/publication/346493744

[19] Q. Wang, C. Ji, Y. Wang, J. Qiang, and C. Dong, "β-Ti Alloys with Low Young's Moduli Interpreted by Cluster-Plus-Glue-Atom Model," *Metallurgical and Materials Transactions A*, vol. 44, no. 4, pp. 1872–1879, Apr. 2013, doi: 10.1007/s11661-012-1523-8.

[20] N. Muchavi, L. Raganya, R. Machaka, G. Motsi, and E. Makhatha, "INFLUENCE OF Sn ON THE MICROSTRUCTURE AND MECHANICAL PROPERTIES OF Ti-Mo-Nb ALLOYS FOR ORTHOPAEDIC APPLICATIONS," *South African Journal of Industrial Engineering*, vol. 33, no. 3, pp. 318–325, 2022, doi: 10.7166/33-3-2806.

[21] M. L. Raganya, "Design of Ti-Mo-Nb-Zr alloys with low elastic modulus using cluster-plus-glue atom model," 2020.

[22] F. Jiang, C. Pang, Z. Zheng, Q. Wang, J. Zhao, and C. Dong, "First-Principles Calculations for Stable β-Ti–Mo Alloys Using Cluster-Plus-Glue-Atom Model," *Acta Metallurgica Sinica (English Letters)*, vol. 33, no. 7, pp. 968–974, Jul. 2020, doi: 10.1007/s40195-020-01006-2.

[23] C. Dong *et al.*, "From clusters to phase diagrams: Composition rules of quasicrystals and bulk metallic glasses," *Journal of Physics D: Applied Physics*, vol. 40, no. 15. Aug. 08, 2007. doi: 10.1088/0022-3727/40/15/R01.

[24] B. Jiang *et al.*, "Effects of Nb and Zr on structural stabilities of Ti-Mo-Sn-based alloys with low modulus," *Materials Science and Engineering A*, vol. 687, pp. 1–7, Feb. 2017, doi: 10.1016/j.msea.2017.01.047.

[25] Q. Wang *et al.*, "Microstructures and Stability Origins of β-(Ti,Zr)-(Mo,Sn)-Nb Alloys with Low Young's Modulus," *Metallurgical and Materials Transactions A*, vol. 46, no. 9, pp. 3924–3931, Sep. 2015, doi: 10.1007/s11661-015-3011-4.

[26] Q. Wang, C. Ji, Y. Wang, J. Qiang, and C. Dong, "β-Ti alloys with low young's moduli interpreted by cluster-plus-glue-atom model," *Metall Mater Trans A Phys Metall Mater Sci*, vol. 44, no. 4, pp. 1872–1879, Apr. 2013, doi: 10.1007/s11661-012-1523-8.

[27] C. Pang, B. Jiang, Y. Shi, Q. Wang, and C. Dong, "Cluster-plus-glue-atom model and universal composition formulas [cluster](glue atom)x for BCC solid solution alloys," *J Alloys Compd*, vol. 652, pp. 63–69, Dec. 2015, doi: 10.1016/j.jallcom.2015.08.209.

[28] S. Ozan, J. Lin, Y. Li, and C. Wen, "New Ti-Ta-Zr-Nb alloys with ultrahigh strength for potential orthopedic implant applications," *J Mech Behav Biomed Mater*, vol. 75, pp. 119–127, Nov. 2017, doi: 10.1016/j.jmbbm.2017.07.011.

[29] J. Lin *et al.*, "Effects of solution treatment and aging on the microstructure, mechanical properties, and corrosion resistance of a β type Ti–Ta–Hf–Zr alloy," *RSC Adv*, vol. 7, no. 20, pp. 12309–12317, 2017, doi: 10.1039/C6RA28464G.

[30] T. Zhou, G. Itoh, Y. Motohashi, and M. Niinomi, "Microstructural Modification in a Beta Titanium Alloy for Implant Applications."

[31] X. H. Min, K. Tsuzaki, S. Emura, and K. Tsuchiya, "Heterogeneous twin formation and its effect on tensile properties in Ti-Mo based β titanium alloys," *Materials Science and Engineering A*, vol. 554, pp. 53–60, Sep. 2012, doi: 10.1016/j.msea.2012.06.009.

[32] S. Emura, X. Ji, X. Min, and K. Tsuchiya, "Effects of Mo segregation on Charpy absorbed energy in Ti-12Mo alloys," *MATEC Web of Conferences*, vol. 321, p. 11050, 2020, doi: 10.1051/matecconf/202032111050.

[33] J. Ruzic, S. Emura, X. Ji, and I. Watanabe, "Mo segregation and distribution in Ti–Mo alloy investigated using nanoindentation," *Materials Science and Engineering A*, vol. 718, pp. 48–55, Mar. 2018, doi: 10.1016/j.msea.2018.01.098.

[34] X. Liu, G. Feng, Y. Zhou, and Q. Fan, "Macrosegregation and the underlying mechanism in Ti-6.5Al-1.0Cr-0.5Fe-6.0Mo-3.0Sn-4.0Zr alloy," *Progress in Natural Science: Materials International*, vol. 29, no. 2, pp. 224–230, Apr. 2019, doi: 10.1016/j.pnsc.2019.02.006.

[35] M. Bönisch *et al.*, "Giant thermal expansion and α-precipitation pathways in Ti-Alloys," *Nat Commun*, vol. 8, no. 1, pp. 1–9, 2017, doi: 10.1038/s41467-017-01578-1.

[36] E. Hildyard, "An investigation into the influence of microstructural condition on the superelastic behaviour in Ti-Nb-based alloys .," University of Cambridge, 2019.

[37] N. Moshokoa, L. Raganya, B. A. Obadele, R. Machaka, and M. E. Makhatha, "Microstructural and mechanical properties of Ti-Mo alloys designed by the cluster plus glue atom model for biomedical application," *The International Journal of Advanced Manufacturing Technology*, pp. 1237–1246, 2020, doi: 10.1007/s00170-020-06208-7/Published.

[38] P. E. L. Moraes, R. J. Contieri, E. S. N. Lopes, A. Robin, and R. Caram, "Effects of Sn addition on the microstructure, mechanical properties and corrosion behavior of Ti-Nb-Sn alloys," *Mater Charact*, vol. 96, pp. 273–281, 2014, doi: 10.1016/j.matchar.2014.08.014.

[39] J. R. S. Martins, R. O. Araújo, R. A. Nogueira, and C. R. Grandini, "Internal friction and microstructure of ti and ti-mo alloys containing oxygen," *Archives of Metallurgy and Materials*, vol. 61, no. 1, pp. 25–30, 2016, doi: 10.1515/amm-2016-0011.

[40] P. Fernandes *et al.*, "Fabrication of low-cost beta-type Ti – Mn alloys for biomedical applications by metal injection molding process and their mechanical properties," vol. 59, pp. 497–507, 2016, doi: 10.1016/j.jmbbm.2016.02.035.

[41] R. Jha and G. S. Dulikravich, "Discovery of new Ti-based alloys aimed at avoiding/minimizing formation of α" and ω-phase using calphad and artificial intelligence," *Metals (Basel)*, vol. 11, no. 1, pp. 1–15, 2021, doi: 10.3390/met11010015.

[42] F. Xie, H. Yang, J. Huang, J. Yu, and X. He, "Sn Content Effects on Microstructure, Mechanical Properties and Tribological Behavior of Biomedical Ti-Nb-Sn Alloys Fabricated by Powder Metallurgy," *Metals (Basel)*, vol. 12, no. 2, Feb. 2022, doi: 10.3390/met12020255.

[43] Y. L. Hao, S. J. Li, S. Y. Sun, and R. Yang, "Effect of Zr and Sn on Young's modulus and superelasticity of Ti-Nb-based alloys," *Materials Science and Engineering A*, vol. 441, no. 1–2, pp. 112–118, Dec. 2006, doi: 10.1016/j.msea.2006.09.051.

[44] D. C. Zhang, S. Yang, M. Wei, Y. F. Mao, C. G. Tan, and J. G. Lin, "Effect of Sn addition on the microstructure and superelasticity in Ti – Nb – Mo – Sn Alloys," *J Mech Behav Biomed Mater*, vol. 13, pp. 156–165, 2012, doi: 10.1016/j.jmbbm.2012.04.017.